NRC·CNRC

NRC Publications Archive
Archives des publications du CNRC

Added value of convection permitting climate modelling in urban overheating assessments

Shu, Chang; Gaur, Abhishek; Wang, Liangzhu (Leon); Bartko, Michal; Laouadi, Abdelaziz; Ji, Lili; Lacasse, Michael

This publication could be one of several versions: author's original, accepted manuscript or the publisher's version. / La version de cette publication peut être l'une des suivantes : la version prépublication de l'auteur, la version acceptée du manuscrit ou la version de l'éditeur.
For the publisher's version, please access the DOI link below./ Pour consulter la version de l'éditeur, utilisez le lien DOI ci-dessous.

Publisher's version / Version de l'éditeur:
https://doi.org/10.1016/j.buildenv.2021.108415
Building and Environment, 207, Part A, 2021-10-05

NRC Publications Archive Record / Notice des Archives des publications du CNRC :
https://nrc-publications.canada.ca/eng/view/object/?id=bcd82f67-e020-48f5-8263-6e038012ad33
https://publications-cnrc.canada.ca/fra/voir/objet/?id=bcd82f67-e020-48f5-8263-6e038012ad33

Access and use of this website and the material on it are subject to the Terms and Conditions set forth at
https://nrc-publications.canada.ca/eng/copyright
READ THESE TERMS AND CONDITIONS CAREFULLY BEFORE USING THIS WEBSITE.

L'accès à ce site Web et l'utilisation de son contenu sont assujettis aux conditions présentées dans le site
https://publications-cnrc.canada.ca/fra/droits
LISEZ CES CONDITIONS ATTENTIVEMENT AVANT D'UTILISER CE SITE WEB.

Questions? Contact the NRC Publications Archive team at PublicationsArchive-ArchivesPublications@nrc-cnrc.gc.ca. If you wish to email the authors directly, please see the first page of the publication for their contact information.

Vous avez des questions? Nous pouvons vous aider. Pour communiquer directement avec un auteur, consultez la première page de la revue dans laquelle son article a été publié afin de trouver ses coordonnées. Si vous n'arrivez pas à les repérer, communiquez avec nous à PublicationsArchive-ArchivesPublications@nrc-cnrc.gc.ca.

National Research Council Canada | Conseil national de recherches Canada

Canada

Added Value of Convection Permitting Climate Modelling in Urban Overheating Assessments

Author names and affiliations

Chang Shu[a,*], Abhishek Gaur[b], Liangzhu (Leon) Wang[a], Michal Bartko[b], Abdelaziz Laouadi[b], Lili Ji[a], Michael Lacasse[b]

[a] Department of Building, Civil and Environmental Engineering, Concordia University, Montreal, 1455 De Maisonneuve, H3G 1M8, Montreal, Quebec, Canada
[b] Construction Research Centre, National Research Council Canada, 1200 Montreal Road, K1A 0R6, Ottawa, Ontario, Canada

***Corresponding author**

Chang Shu;
PhD Candidate
Department of Building, Civil & Environmental Engineering
Concordia University
Ev.BLDG 014.169
1455 De Maisonneuve Blvd. W.
Montreal, Quebec, Canada
H3G 1M8
+1 (514)-575-0218
Email: *changshu769@gmail.com*

Added Value of Convection Permitting Climate Modelling in Urban Overheating Assessments

Authors: Chang Shu, Abhishek Gaur, Liangzhu (Leon) Wang, Michal Bartko, Abdelaziz Laouadi, Lili Ji, Michael Lacasse

Abstract

As a consequence of global warming and rapid urbanization around the globe, the magnitudes and frequencies of extreme heat events (EHEs) are increasing and this trend is expected to continue into the future. In this study, the added benefit of modelling climate at convection-permitting spatial resolutions (grid spacing < 4 km) is considered for a set of exterior climate and interior building simulations during EHEs in the urban areas of Ottawa and Montreal, Canada over the summer of 2018. The climate is modelled at two spatial resolutions: i) 25 km – typically considered for regional-scale climate modelling; and ii) 1 km. The results derived from modeling at each of these resolutions is compared in respect to their adequacy in predicting different measures of overheating outdoors as well as those within a typical single-detached home. The results clearly demonstrate that simulations undertaken at a 1 km resolution permit more accurately calculate the magnitude of overheating, whereas simulations completed at a 25 km resolution lead to an underestimation of overheating in about 95% of the urban grids within either of these two cities. These results suggest the necessity of using convection-permitting climate simulations for overheating assessments over the urban scale.

Keywords

Weather Research and Forecasting, Overheating, Extreme heat event, Urban heat island, EnergyPlus, Heatwave

Highlights

- Urban climate of Ottawa and Montreal is simulated at 1 and 25 km spatial resolutions.
- Added value of convection-permitting model in overheating studies is demonstrated.
- Simulations at a high-resolution are found more accurate in simulating urban temperatures and wind.
- Use of regional climate simulations leads to underestimation of overheating.

1. Introduction

As a consequence of global warming and urban expansion, the frequency and intensity of extreme heat events (EHEs) in cities around the globe is increasing, resulting in both high morbidity and mortality [1–4]. Urban areas are typically warmer, wetter, and less windy than the areas surrounding them due to their distinct morphology [5]. This urban-rural climate contrast cannot be properly simulated by global climate models (GCMs) operating at a spatial resolution of 100-300 km, and typically a downscaling step is required to complete a useful simulation.

A limited-area regional climate model (RCM) performs dynamic downscaling of GCMs and produces regional-scale climate estimates at 10-50 km spatial resolution [6]. State-of-the-art reanalysis datasets such as ERA-Interim [7], North American Regional Reanalysis [8] and the Climate Forecast System Reanalysis [9] , also provide regional-scale estimates of historical climate at aforementioned spatial resolutions. The RCMs add value over the GCMs for three reasons: i)

the finer resolution allows a more realistic representation of surface forcings such as orography, lakes, rivers, and coastal regions; ii) the finer resolution allows a more accurate discretization of equations, and thus, a better simulation of the atmospheric circulation and gradients; and iii) with finer resolution, a broader range of fine-spatial scale processes can be explicitly resolved, which includes mesoscale weather phenomena such as sea breezes, lake-effect snowstorms, local winds, tropical cyclones and mesoscale convective systems [10].

Several studies have investigated the benefit or "added value" [11] of modelling climate at finer regional scales. Lucas-Picher et al. [12] compared climate across North America over 1979-2014 as simulated by the Canadian Regional Climate Model version 5 (CRCM5) [13,14] at 0.44°, 0.22°, and 0.11° spatial resolutions. They concluded that higher spatial resolution simulations showed a more realistic description of complex climate phenomena as orographic precipitation, precipitation extremes, sea-breeze formulation, and similar climate phenomena. Similarly, Qiu et al. [15] compared climate simulations performed at 20 km and 5 km over South Korea over a 20-year historical period and concluded that both sets of climate simulations captured the spatially and temporally averaged climate characteristics. Meanwhile, finer scale simulations better simulated the intensity and frequency of extreme events and spatio-temporal variations in climate variables. Mayer et al. [16] discussed the importance of performing high-resolution climate simulations for assessing the impacts of extreme events on infrastructure by comparing 8 km resolution simulation results with lower resolution simulations conducted at about 70 km over Scandinavia. On the other hand, Curry et al. [17] identified limited added value of 15 km resolution simulations over 45 km resolution simulations from Canadian Regional Climate Model version 4 [18] in terms of predicted temperature and precipitation. It was concluded that the added value by RCMs depends on the variable to be evaluated and the problem to be addressed.

Convection permitting models (CPMs) are a type of regional climate models (RCMs) in which climate simulations are conducted at a spatial resolution of less than 4 km. CPMs offer more accurate climatic information for regional to local scale applications than RCMs because they do not require convection parameterization, which identified as a major source of errors and uncertainties in the RCMs. At the same time, they allow for an even more accurate representation of surface and orographic fields in the simulations [19]. Several studies have used CPMs to obtain local scale climate using boundary conditions from GCMs [20,21] or RCMs [22–24]. The CPMs have been found to add value over RCMs in simulating mean precipitation [25–27], their spatial patterns[22,23], and extremes [24,27,28]. Similar improvements in the modeling of temperature and its extremes have been obtained [23,29]. Meanwhile, their added value has also been demonstrated in local-scale impact assessments, for instance, in the simulations of the energy and mass balance of glaciers [30], river runoff, and flood forecasting [31,32], and renewable energy production [33–35].

CPMs have been used to model urban climate, assess the effects of urbanization and climate change in urban areas, and evaluate the effectiveness of various heat-stress mitigation strategies. Weverberg et al. [36] isolated the contribution of urban heat island (UHI) on temperatures recorded in Uccle, Belgium, by conducting 1 km resolution simulations using the Weather Research and Forecasting (WRF) model [37] and comparing them with the observational records. The role of urban growth in forming four historical EHEs in the Phoenix, Arizona metropolitan area was evaluated by Grossman-Clarke et al. [38]. It was found that new urban developments around the city caused an intensification and expansion of the area experiencing extreme temperatures during EHE. Wouters et al. [39] simulated the UHI over Paris by conducting 1 km resolution urban climate simulations using an Advanced Regional Prediction System [40,41]. Taha

[42] demonstrated that UHI could be mitigated by up to 3ºC in Sacramento by increasing the city's albedo and urban vegetation cover. Schubert and Grossman-Clarke [43] demonstrated the effectiveness of increasing green urban infrastructure, high-reflective surfaces, and judicious selection of building materials in effectively reducing the heat stress in Berlin, Germany, during EHE.

The external climate is a significant driver of a building's indoor conditions. A few recent studies have used climate simulated by CPMs in simulating the indoor environment in buildings. Ciancio et al. [44] simulated the climate of the metropolitan area of Rome by performing a 4 km resolution WRF simulation. The simulated outdoor conditions were used to undertake building energy simulations in EnergyPlus [45]. The results were compared with another two simulations using the weather data recorded at airports. The study concluded that using the weather data from airports might result in an underestimation of cooling energy consumption and an overestimation of heating energy consumption in the city as urban effects are not accounted for. Similar conclusions were drawn by Jain et al. [46], who emphasized the importance of using climate data with urban effects incorporated, which can be simulated in a WRF simulation, for the prediction of building energy in Chicago. Luo et al. [47] evaluated the spatial variation of the building waste heat emission in Los Angeles, California, by conducting WRF simulations at 500m spatial resolution and building energy simulations using EnergyPlus. It was concluded that heat emission from the buildings during EHEs exacerbates the outdoor heat stress, especially in densely populated urban districts in the city.

Previous studies have used high-resolution climate simulations using CPMs for building simulations, while they only focused on studying the building’s impact on the outdoor environment and/or evaluating the building energy consumptions.The added value of CPMs over RCMs has not

been quantified in a building overheating context. This study fills this research gap by comparing two sets of simulations of an extreme summer season recorded in the Ottawa and Montreal region of Canada. The first set of simulations is conducted at a typical RCM spatial scale (25 km), and the second at a CPM scale (1 km). The results from this study provide evidence and novel information that help confirm the importance of using CPMs when assessing overheating in buildings located in urban areas. The rest of the paper is organized as follows: the details of the study area, data, and methods are provided in section 2, followed by results and discussion in section 3, and conclusions in section 4.

2. Methodology

2.1 Study area and evaluation period

The study area comprises of two Canadian cities: Ottawa, in the province of Ontario, and Montreal in the province of Quebec (Figure 1). The region encompassing these cities experienced an extreme heat event (EHE) from June 30 – July 05, 2018, resulting in around 70-100 heat-related deaths in both provinces [48]. During this EHE, parts of Ottawa reached an all-time highest humidex [49] value of 47, and the city of Montreal's public health office recorded 66 heat-related deaths in the city [50]. The city-scale overheating of the two cities is evaluated over the five months of Summer 2018 (May 01 – September 30), encompassing the EHE.

Figure 1. The numerical domain in WRF simulation surrounding the geographical location of the study area and the two cities, Ottawa and Montreal.

The layout of the two cities used in the WRF simulations can be seen from Figure 2, which shows the distribution of the land use and land cover (LULC) surrounding the two cities from the 2015 North American Land Change Monitoring System (NALCMS) dataset [51]. The urban areas are represented in the WRF model by the means of a single urban class because our previous work showed that using more than one categories of urban land-cover in the cities didn't add any value in the WRF model in terms of it's accuracy in modelling urban climate parameters in these cities. The Ottawa river passes through the north of the city. On the other hand, the layout of the urban area in Montreal is quite different. The center of the city is located on Montreal Island, which is

surrounded by rivers. There are also several small agglomerations of urban areas outside the island. Both cities are surrounded by croplands and forested areas. The study area normally experiences a semi-continental climate, with warm, humid summers and cold winters.

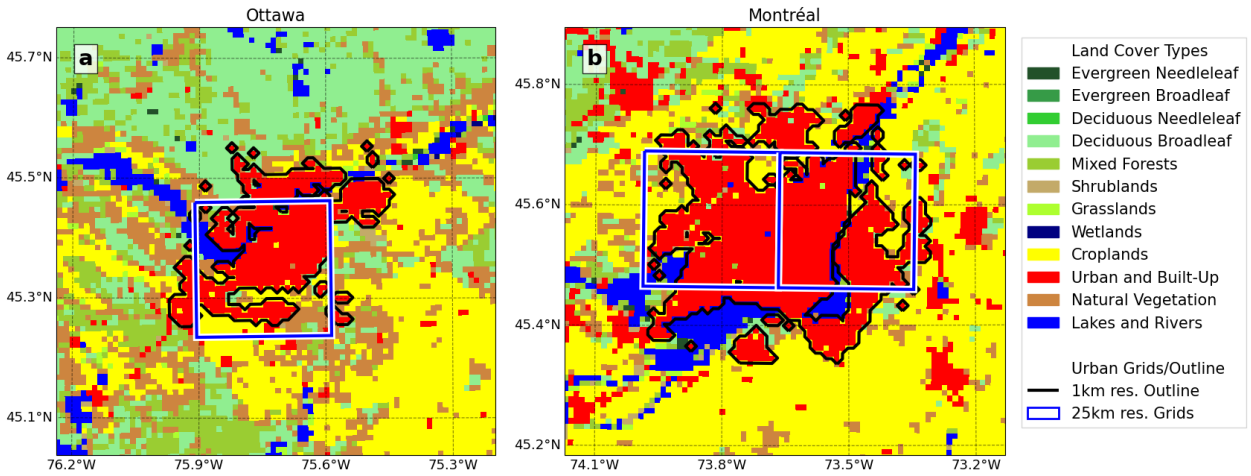

Figure 2. Land use and land cover (LULC) around a) Ottawa and b) Montreal cities and the outlines of urban area considered in 1 and 25 km resolution climate simulations.

2.2 Weather Research and Forecasting (WRF) configurations

The regional climate model used in this study is the Weather Research and Forecasting (WRF) model [37]. The National Centres for Environmental Prediction (NCEP) North American Regional Reanalysis (NARR) product # ds608.0 [52] are used as the initial and boundary conditions for the WRF simulations. The setup of the simulations completed at a 1 km-resolution consists of three two-way nested domains with 276 × 296, 250 × 283, and 391 × 364 grid points at a grid distance of 9, 3, and 1 km, respectively. For simulations completed at the 25 km-resolution, only one non-nested domain is used with 100 × 100 grid points, covering a similar area (shown as the dotted blue line in Figure 1) as the first parent domain in the simulation completed at a 1 km-resolution

(shown as the solid black line in Figure 1). The domains for both sets of simulations are centered in the middle of the Ottawa and Montreal cities (74.63°W, 45.47°N).

A series of WRF simulations were conducted in our previous study to evaluate the performances of using different urban parametrizations and LULC datasets and identify optimum settings for the modelling of urban climate in the two cities [53]. The model configuration listed in Table 1 simulated urban climate in the cities with the best accuracy are therefore adopted in this study as well. Note that the cumulus parameterization is only activated for simulations completed at the 25 km resolution and the first domain with a grid spacing of 9 km in the simulation completed at the 1 km resolution. In comparison, the model of the second and third domains with a grid spacing of 3 km and 1 km can resolve the deep convection as the grids are smaller than 4 km.

Table 1. Physical parameterization schemes in WRF simulations.

Category	Physical parameterization scheme
Microphysics	WRF Single-Moment 3-class scheme (WSM3) [54]
Land Surface model	NOAH [55]
Planetary boundary layer	Two-order closure Mellor-Yamada-Janjic [56]
Shortwave radiation	Dudhia scheme [57]
Longwave radiation	Rapid Radiative Transfer Model (RRTM)[58]
Cumulus parameterization	Kain-Fritsch scheme [59] for domains of grid size > 4 km
Advection scheme	Runge-Kutta 3rd order
Land cover classification	MODIS 21-category
Number of vertical layers	40
Urban canopy model	Multilayer UCM building effect parametrization (BEP) [60]

2.3 Climate observations

The WRF model is validated over the time period of analysis, i.e., May-September, 2018 with regards to its performance in simulating observed values of climate variables: air temperature, and wind speed, as recorded at Environment and Climate Change Canada (ECCC) operated climate

gauging stations surrounding the cities of Ottawa and Montreal. The observations of hourly climate are collected from ECCC historical climate database [61]. Nine climate gauging stations are located around the two cities and contain the hourly observations of the variables that are used for analysis. These ECCC stations and their local LULC types are listed in Table 2, and their locations are shown in Figure A1 of the appendix.

Table 2. Details of climate gauging stations for WRF model evaluation.

Short Name	Full Name (Province)	Latitude (°N)	Longitude (°E)	Local LULC type
GATI	Ottawa Gatineau A (Québec)	45.52	-75.56	Croplands
OTUB	Ottawa Cda Rcs (Ontario)	45.38	-75.72	Urban and Built-up
OTAP	Ottawa Intl A (Ontario)	45.32	-75.67	Urban and Built-up
MIRA	Montreal Mirabel Intl A (Québec)	45.68	-74.04	Urban and Built-up
SHUB	Montreal/St-Hubert (Québec)	45.52	-73.42	Urban and Built-up
MCTA	McTavish (Québec)	45.50	-73.58	Urban and Built-up
PETR	Montreal/Pierre Elliott Trudeau Intl (Québec)	45.47	-73.75	Croplands
INTL	Montreal Intl A (Québec)	45.47	-73.74	Urban and Built-up
ANNE	Ste-Anne-De-Bellevue 1(Québec)	45.43	-73.93	Croplands

2.4 Building simulation model

Previous studies have found that most of the heat-related deaths in the 2018 EHE happened in residential buildings [50]. In this study, a typical residential building type: a single-detached home, is selected for the assessment. A building model of the archetype single-detached home [62], shown in Figure 3, is prepared in EnergyPlus [45]. The building model comprises of four thermal zones: the underground basement, living room on the first floor, bedroom on the second floor, and an attic on the top of the building. The total footprint area of the building is 80.20 m^2. In Table 3, the building envelope configurations are listed, following the current construction practice [63] for homes. The internal heat gains and schedules also follow recommendations taken from the National Building Code of Canada [63], with 5 W/m^2 for lighting, 5 W/m^2 for equipment, and

500 $W/person$ for the servicing of hot water. The occupancy of the building is considered for a typical family of three people. For the building infiltration rate, an air change rate of 2.32 air changes per hour at 50 Pa obtained from a measurement database for new homes of the region is considered for the current construction. The building model is naturally ventilated for the evaluation of the potential overheating under a free-running condition following the requirements of the overheating guidelines [64]. Natural ventilation (open window) is available when the outdoor air temperature is lower than the indoor air temperature, and the indoor air temperature is higher than 26°C [63]. The occupant schedules for the living room were defined as 7:00 to 21:00 hours and 22:00 to 6:00 hours for the bedroom according to the most recent versoin of the National Energy Code of Canada for Buildings (NECB) [65].

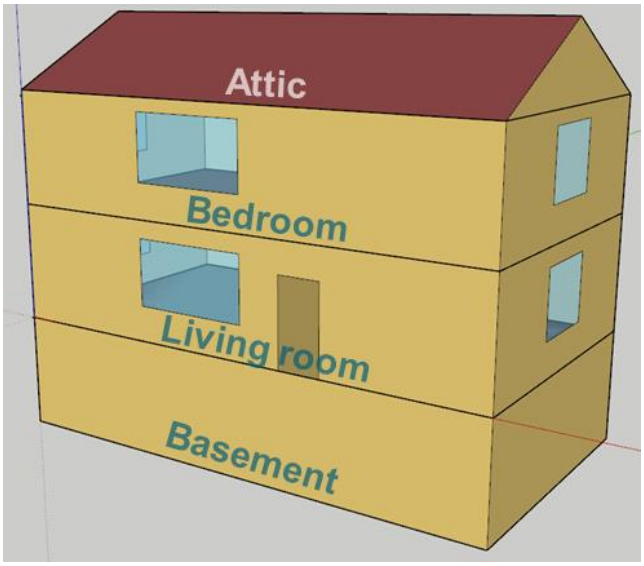

Figure 3. Archetype single-detached home building model used for indoor overheating analysis using EnergyPlus.

The climate inputs for EnergyPlus simulations are prepared from WRF outputs from (1 or 25 km resolution) grids closest to the locations of interest. The climate varibles considered from WRF

simulations are: dry bulb air temperature, dew point temperature, relative humidity, atmospheric station pressure, global horizontal radiation, wind speed and wind direction, cloud fraction, rain fall and snow depth. In addition, the global horizontal radiation is used to estimate direct horizontal irradiance, direct normal irradiance, and diffused horizontal irradiance using widely used methods [66].

Table 3. Envelope components for building model of archetype single-detached home

Component	Material and properties
Window	Double clear with Low-E (U = 1.58; VT = 73%; SHGC = 0.67, WWR =15%)
Roof	Asphalt shingles with attic insulation (RSI 8.2)
Walls	Wood stud with Vinyl cladding (RSI 4.5)
Basement Wall	Insulated concrete (RSI 1.7)
Basement Slab	Insulated concrete (RSI 1.6)
Blinds	Internal blinds

2.5 Overheating assessment

There is no universal definition and criteria for defining EHE for overheating assessments [67]. A literature review of previous studies has shown that a fixed or adaptive temperature threshold value can be chosen to identify overheating events [67–69]. In this study, a fixed temperature threshold is used for overheating assessment since it has been widely used in previous overheating studies, standards, and codes, and is more suitable for our application, i.e., to compare climate simulations at multiple spatial resolutions. Following the practical guidelines of extreme weather file selection [70] and indoor overheating evaluation [64], the threshold value for outdoor overheating is chosen as 28°C, and for indoor overheating, the used temperature thresholds are 28°C for the living room, and 26°C for the bedroom. Furthermore, operative temperature (T_{opt}), which better reflects the

thermal sensation of occupants, is used for indoor overheating evaluation. These values have also been adopted by other standards, codes and guidelines [71–73].

The hours with air temperature or indoor operative temperature higher than the above thresholds are defined as overheating hours (OH) and are used to calculate the percentage of overheating (POH) durations using the total number of hours over the evaluation period (e.g. 3672 h in total for May-September 2018). To segregate indoor overheating in different building spaces, the percentage of overheating hours is calculated for the daytime and nighttime, assuming occupancy of the living room in the daytime (7 AM to 9 PM) and bedrooms in the nighttime (10 PM to 6 AM). The mean air/operative temperature and maximum air/operative temperature are also calculated to quantify overheating.

3. Results and discussions

3.1. Accuracy of simulations completed at 25 and 1 km grid resolution

The accuracy of the modelled near-surface climate variables from simulations completed at 25 and 1 km resolution is quantified by comparing the simulated data with the hourly measurements from nine weather stations surrounding the Ottawa and Montreal cities. The root mean square error (RMSE), mean absolute error (MAE) and mean bias error (MBE) associated with the simulation results are calculated using Equations 1-3.

$$RMSE = \sqrt{\frac{\sum_{i=1}^{N}(x_{m,i}-x_{o,i})^2}{N}} \quad (1)$$

$$MAE = \frac{\sum_{i=1}^{N}|x_{m,i}-x_{o,i}|}{N} \quad (2)$$

$$MBE = \frac{\sum_{i=1}^{N}(x_{m,i}-x_{o,i})}{N} \quad (3)$$

where i corresponds to each time step in the evaluation, N is the total number of hours, and $x_{m,i}$ and $x_{o,i}$ are the simulated and measured values, respectively.

From the results summarized in Table 4, it is clear that RMSE and MAE associated with simulations completed at a 1 km resolution are lower than those at a 25 km resolution for both air temperature and wind speed. The MBE of air temperature from simulations completed at a 1 km and 25 km resolution are negative, indicating that air temperatures are underestimated for both simulations. The MBE ranged from -0.4 ºC to -2.0 ºC for temperatures derivied from simulations of 1 km resolution and -1.4 ºC to -2.6 ºC for those at a 25 km resolution, showing the magnitude of underestimation is lower for simulations completed at 1 km resolution than those at 25 km resolution. The MBE of wind speed varies between negative and positive values for different weather stations, reflecting the complex and highly variable nature of the wind speed variable. The MBE of wind speed from the 1 km resolution model varies between -1.4 m/s to 1 m/s, whereas MBE from the 25 km resolution model varies from -1.3 m/s to 1.5 m/s, indicating higher accuracy of simulations completed at a 1 km as compared to 25 km resolution.

Table 4. Root Mean Square Error (RMSE), Mean Absolute Error (MAE), and Mean Bias Error (MBE) of the simulated near-surface variables: air temperature and wind speed.

Criteria	Variables	Resolution	GATI	OTUB	OTAP	MIRA	SHUB	MCTA	PETR	INTL	ANNE	Avg.
RMSE	Air Temperature (°C)	1 km	2.6	2.5	2.4	2.5	2.4	2.6	3.3	3.0	3.2	2.7
		25 km	3.1	3.0	2.9	2.7	2.8	3.4	3.5	3.4	2.9	3.1
	Wind Speed (m/s)	1 km	1.7	1.5	1.6	1.3	1.9	1.6	1.7	2.2	1.7	1.7
		25 km	2.1	1.4	1.7	2.3	1.9	1.9	1.7	2.1	2.4	2.0
MAE	Air Temperature (°C)	1 km	2.0	2.0	1.9	1.9	1.9	2.1	2.6	2.4	2.6	2.2
		25 km	2.5	2.4	2.3	2.2	2.3	2.8	2.9	2.8	2.4	2.5
	Wind Speed (m/s)	1 km	1.3	1.1	1.2	1.0	1.4	1.3	1.3	1.8	1.3	1.3
		25 km	1.6	1.1	1.3	1.8	1.5	1.5	1.3	1.7	1.9	1.5

MBE	Air Temperature (°C)	1 km	-0.4	-0.8	-0.8	-0.6	-0.8	-1.3	-2.0	-1.8	-1.9	-1.1
		25 km	-1.9	-1.9	-1.8	-1.4	-1.6	-2.4	-2.6	-2.5	-1.7	-2.0
	Wind Speed (m/s)	1 km	0.6	0.3	-0.6	0.3	-0.8	1.0	-0.4	-1.4	0.7	0.0
		25 km	1.1	-0.1	-0.7	1.5	-1.0	1.2	-0.8	-1.3	1.5	0.2

The observed hourly temperatures are also compared with simulation results completed at 1 and 25 km resolution using scatterplots and linear regression analysis. The results are presented for all nine climate gauging stations in Figure 4. The simulation results for the 1 km resolution and trend line (in red) are found to be better aligned with the observations than the temperatures from simulations completed at a 25 km resolution for eight out of nine stations. For one station (ANNE), the results are similar. The distribution of the scatter points illustrates that hourly temperatures from simulations completed at a 25 km resolution are lower than those from 1 kmresolution, especially at higher temperatures. This can be seen from a comparison of the linear regression lines of simulations completed at a 25 km resolution with a greater deviation from observations at higher temperatures than lower temperatures. On the other hand, simulations completed at a 1 km resolution demonstrate a lower level of errors under extreme temperatures showing their higher utility for overheating assessments.

The regression coefficients of both sets of simulations are summarized in Table 5. The simulations completed at 1 km have a higher coefficient of determination (R^2) on average of 0.78 than the 25 km resolution with R^2 of 0.73, showing the 1 km resolution model has a stronger capability for simulating the variance in air temperature. The simulations completed at a 1 km resolution show a stronger positive correlation with the observations (0.97), which is significantly better than those at 25 km resolution (0.93). Also, the simulations completed at 1 km resolution exhibit a lower level of underestimation in air temperature with the averaged intercept of -0.5 comparing to the value of -0.64 from the simulations completed at 25 km resolution.

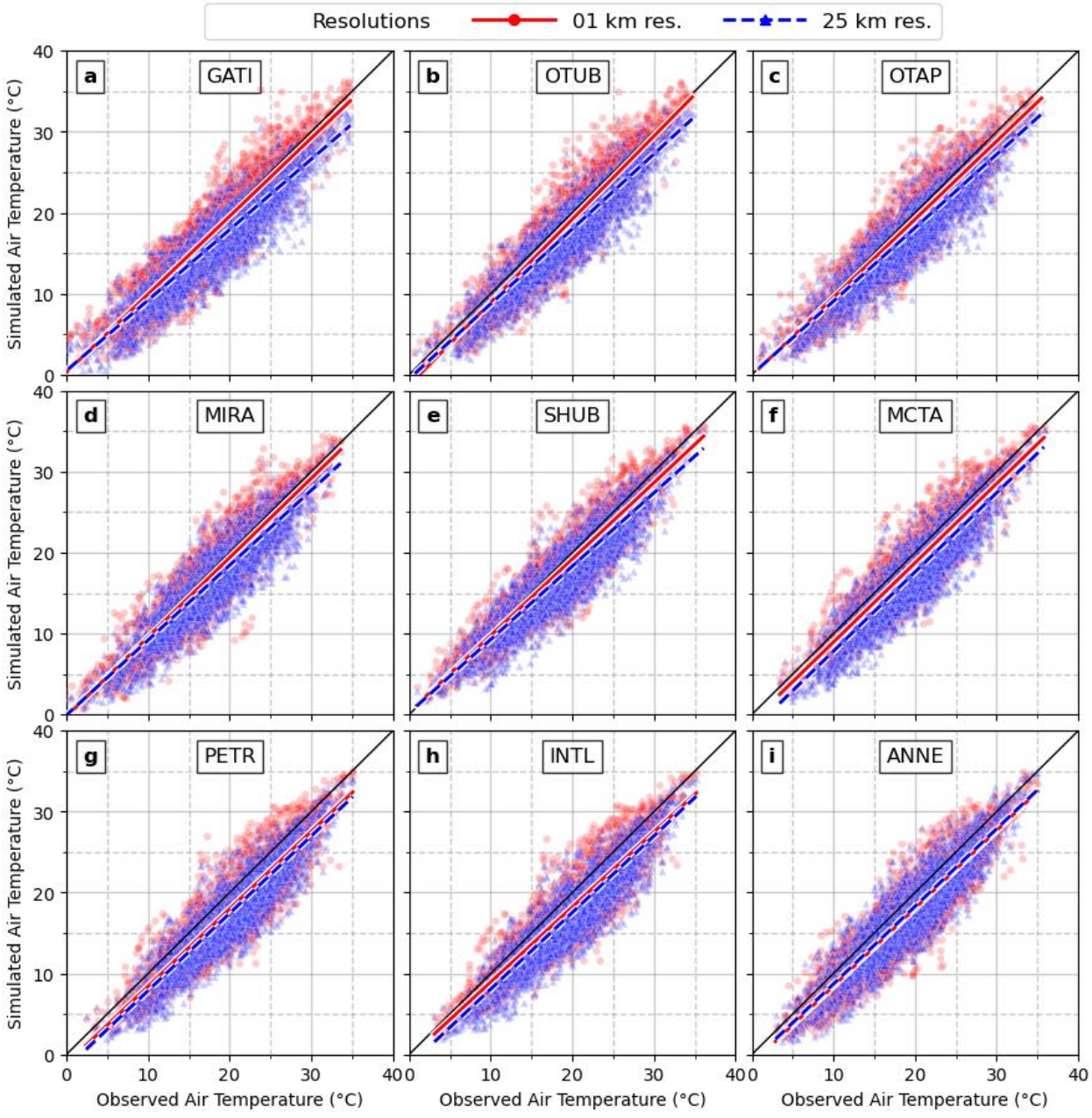

Figure 4. Comparison of the simulated and measured air temperatures from the nine weather stations during the five months (May 01 - September 30) in the summer of 2018. The red solid lines show the correlation between the observation and the WRF simulations completed at 1 km resolution, and the blue dashed lines show the correlation between the observation and the WRF simulations completed at 25 km resolution.

Table 5. Linear regression coefficients between observations and simulations at nine climate gauging stations.

Linear regression coefficients	Station	GATI	OTUB	OTAP	MIRA	SHUB	MCTA	PETR	INTL	ANNE	Average
Slope	1 km res.	0.96	1.03	0.97	0.98	0.94	0.98	0.96	0.93	0.96	0.97
	25 km res.	0.87	0.93	0.91	0.93	0.91	0.98	0.96	0.95	0.96	0.93
Intercept	1 km res.	0.28	-1.32	-0.11	-0.23	0.34	-0.84	-1.16	-0.33	-1.16	-0.50
	25 km res.	0.48	-0.52	0.00	-0.07	0.22	-1.94	-1.68	-1.38	-0.88	-0.64
R-squared	1 km res.	0.84	0.82	0.85	0.83	0.85	0.67	0.78	0.72	0.70	0.78
	25 km res.	0.76	0.75	0.78	0.79	0.78	0.62	0.64	0.66	0.75	0.73

3.2. Outdoor overheating from simulations completed at 1 and 25 km grid resolution

In addition to being more accurate, the simulations completed at 1 km resolution can capture the spatial distribution of temperature extremes and overheating better within and around the two cities than those at 25 km resolution. This is clear from Figure 5, which shows the distribution of mean air temperature over May-September 2018 obtained from simulations completed at 1 and 25 km resolution. It can be seen that the spatial variation of temperature is better represented in the simulations completed at 1 km resolution, whereas the urban extents of the Ottawa (Montreal) city are encompassed by one (two) simulations completed at 25 km resolution grids. Therefore, urban temperatures, and resulting overheating, are not properly captured by the simulations completed at 25 km resolution. Moreover, the urban-rural differences in climate are not well captured. For example, the lower temperatures over water bodies are not well captured in simulations completed at 25 km resolution, whereas they are better captured in simulations completed at 1 km resolution.

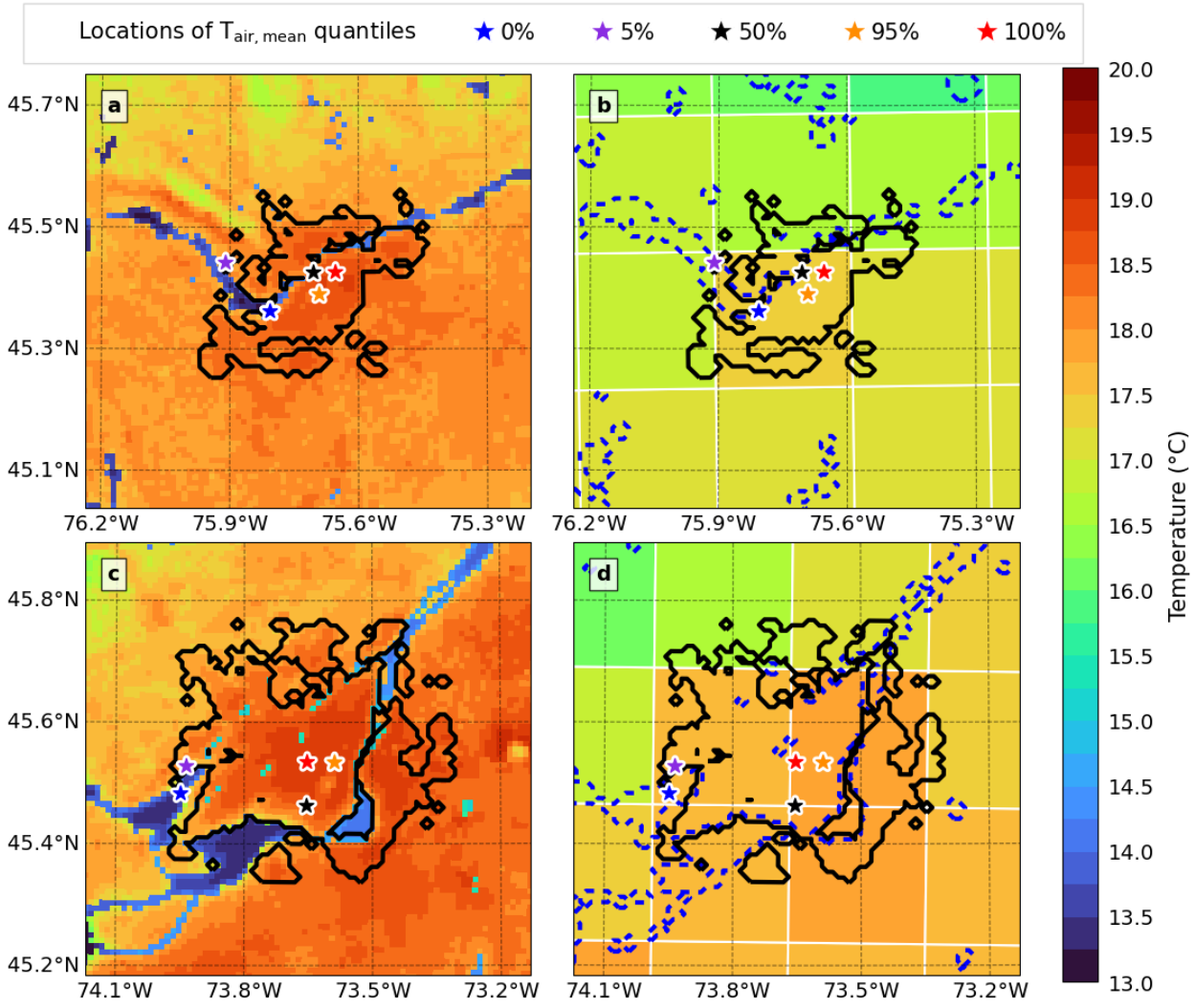

Figure 5. Modelled air temperature distribution averaged over the five months (May - September 2018) around the two cities: Ottawa (a,b) and Montreal (c,d) from simulations completed at 1 km resolution (a,c), and 25 km resolution (b,d).

The temperatures, their extremes, and resulting overheating are generally underpredicted in simulations completed at 25 km resolution over the land areas compared to simulations completed at 1 km resolution. The difference in mean air temperature ($T_{air,mean}$), maximum air temperature ($T_{air,max}$) and overheating hours above 28°C ($OH_{28°C}$) between simulations completed at 1 and 25 km resolution are shown in Figure 6. For the $T_{air,mean}$ (Figure 6 a, d) over May-September

2018, the magnitude of underprediction can be up to 2°C. The underprediction in the case of $T_{air,max}$ can be up to 3°C. Finally the total number of overheating hours are also severely underpredicted (up to 200 hours over five months) in the simulations completed at 25 km resolution as compared to the results simulations completed at 1 km resolution . These results demonstrate that simulations completed at 1 km resolution are more suited to capture the variations in extreme temperatures and the associated overheating conditions than those at 25 km resolution.

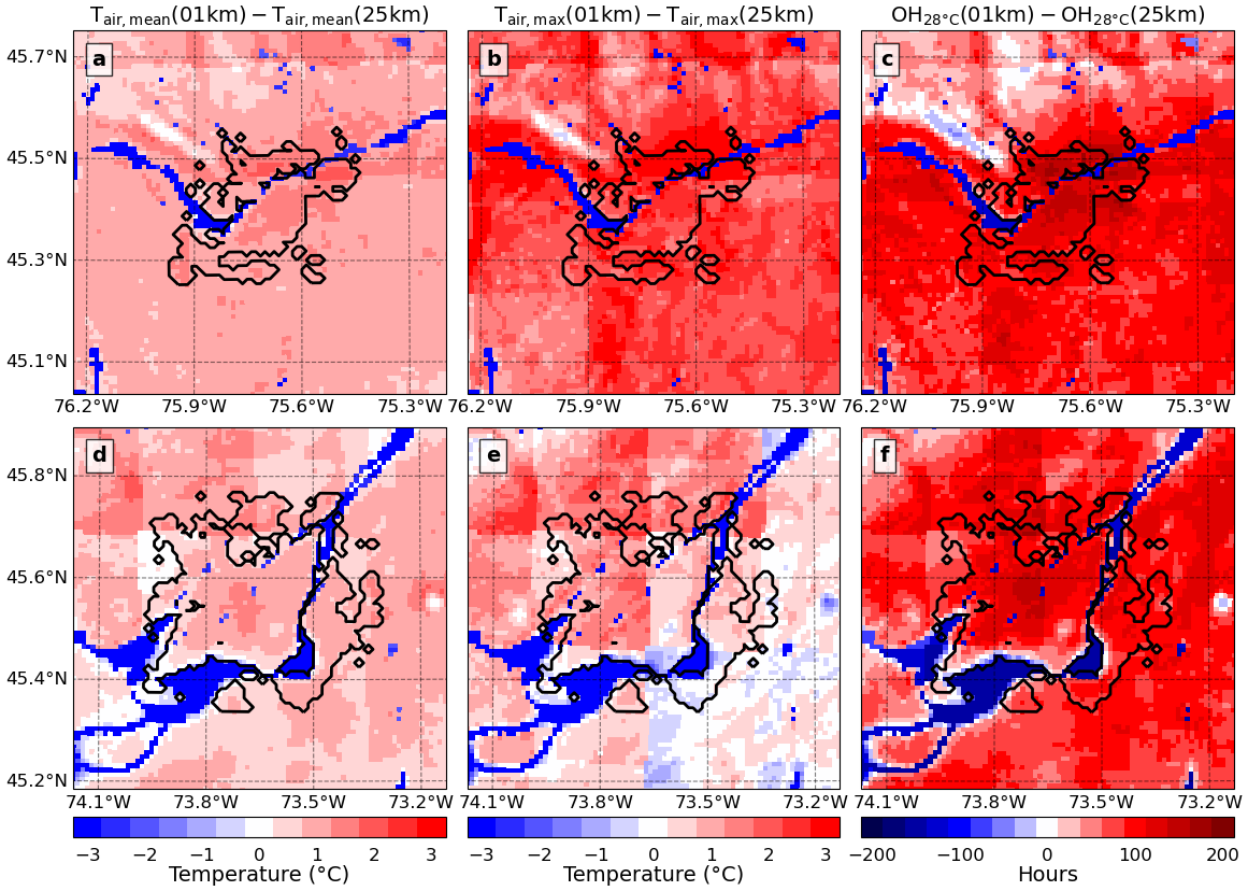

Figure 6. The difference in simulation results completed at 1 km and 25 km grid resolutions over Ottawa (a,b,c) and Montreal (d,e,f) in terms of mean air temperature (a,d), maximum air temperature (b,e) and the number of overheating hours (c,f).

To further investigate the differences in simulated overheating over urban areas from the two simulation groups, five grids from simulations completed at a 1 km resolution are selected in each city for assessment. These grids correspond to 0, 5, 50, 95, and 100th quantiles of simulated mean air temperature over the Summer of 2018 from simulations completed at a 1 km resolution. Hereafter, these grids are referred to the city names (Ottawa or Montreal), data source (fine or coarse resolution results), and quantile values associated with the grid. For example, OF_0 denotes the Ottawa Fine resolution grid with the 0th quantile value in terms of mean temperature. Similarly, the 25 km grid associated with these 1 km grids is referred to the city names (Ottawa or Montreal) and data source (fine or coarse resolution results). For example, OC refers to the Ottawa Coarse grid case. In the case of Montreal, the two grids are named as MC_W (Montreal Coarse grid located on the West) and MC_E (Montreal Coarse grid located on the East). The locations of these representative grids are shown in Figure 5 (1 km simulation grids) and Figure 2 (25 km simulation grids). In the case of Ottawa, all selected 1 km grids fall within one 25 km grid, whereas in the case of Montreal, two 1 km grids are located within MC_W and three 1 km grids are located in MC_E.

The mean ($T_{air,mean}$) and maximum air temperatures ($T_{air,max}$), percentage of overheating hours over 28ºC ($POH_{28^\circ C}$), and mean wind speed (WS_{mean}) for the representative grids are summarized in Table 6. The results show that the mean and extremes of temperature and overheating conditions are highly underestimated in simulations completed at a 25 km resolution. The number of the overheating hours at the 50th percentile 1 km simulation grid is almost twice the value of that at the 25 km simulation grid. In fact, for both cities, the mean and extremes temperatures and overheating hours from simulations completed at a 25 km resolution are always lower than the values associated with the 5th percentile 1 km simulation grid, which means that only 5% of 1 km simulation grids have lower mean and extremes temperatures, and overheating

hours than the 25 km simulation grids. This is also true for the wind speeds where none of the 1 km grids in Ottawa and less than 5% of 1 km simulation grids in Montreal are found to have lower wind speeds than simulations completed at a 25 km resolution.

Table 6. Summary of the outdoor thermal conditions at representative urban grids for simulations completed at 1 km and 25 km grid resolution.

Climate statistic	Ottawa grids						Montreal grids						
	OC	OF_0	OF_5	OF_{50}	OF_{95}	OF_{100}	MC_W	MC_E	MF_0	MF_5	MF_{50}	MF_{95}	MF_{100}
$T_{air,mean}(°C)$	17.3	13.8	17.9	18.4	18.7	18.8	17.5	17.8	13.4	17.7	18.5	18.9	19.0
$T_{air,mean}^{day}(°C)$	19.2	15.0	19.8	20.8	21.0	21.1	19.4	19.7	14.3	19.9	20.7	20.9	21.1
$T_{air,mean}^{night}(°C)$	14.1	11.8	14.8	14.5	14.9	15.0	14.4	14.6	12.0	14.1	15.0	15.6	15.5
$T_{air,max}(°C)$	33.6	25.1	34.9	36.3	36.1	36.1	34.0	35.3	23.8	35.0	35.2	35.9	35.9
$POH_{28°C}$ (%)	3.3	0.0	4.5	7.0	7.1	7.5	3.2	3.8	0.0	4.1	6.0	6.6	7.1
$WS_{mean}(m/s)$	2.9	2.6	2.6	2.3	2.3	2.2	2.8	2.9	3.4	2.2	2.6	2.7	2.4

The hourly distribution of temperatures from simulations completed at a 1 and 25 km resolution and their difference over the analysis time period from May 1 to September 30, 2018 is presented in Figures 7 and 8, respectively, for the 50th percentile location. Figure 7 illustrates that both simulations completed at 1 and 25 km resolutions can capture the much higher temperature occurred during the EHE of June 30 – July 5, 2018 than other days during the evaluated 5 months. However, Figure 8 makes it clear that the intensity of the extreme event is underestimated in the simulations completed at a 25 km resolution, as found in the previous results. For example, during the five months, 69% of hours in Ottawa and 75% of hours in Montreal have a higher temperature than the simulations completed at a 25 km resolution. Another important observation from Figure 8 is that the underprediction of temperatures in simulations completed at a 25 km resolution, which can be as high as 10ºC in some cases, is more prevalent in the daytime than the night-time. A high

overestimation of temperatures of up to 6 ºC is obtained in the simulations completed at a 25 km resolution during the night-time.

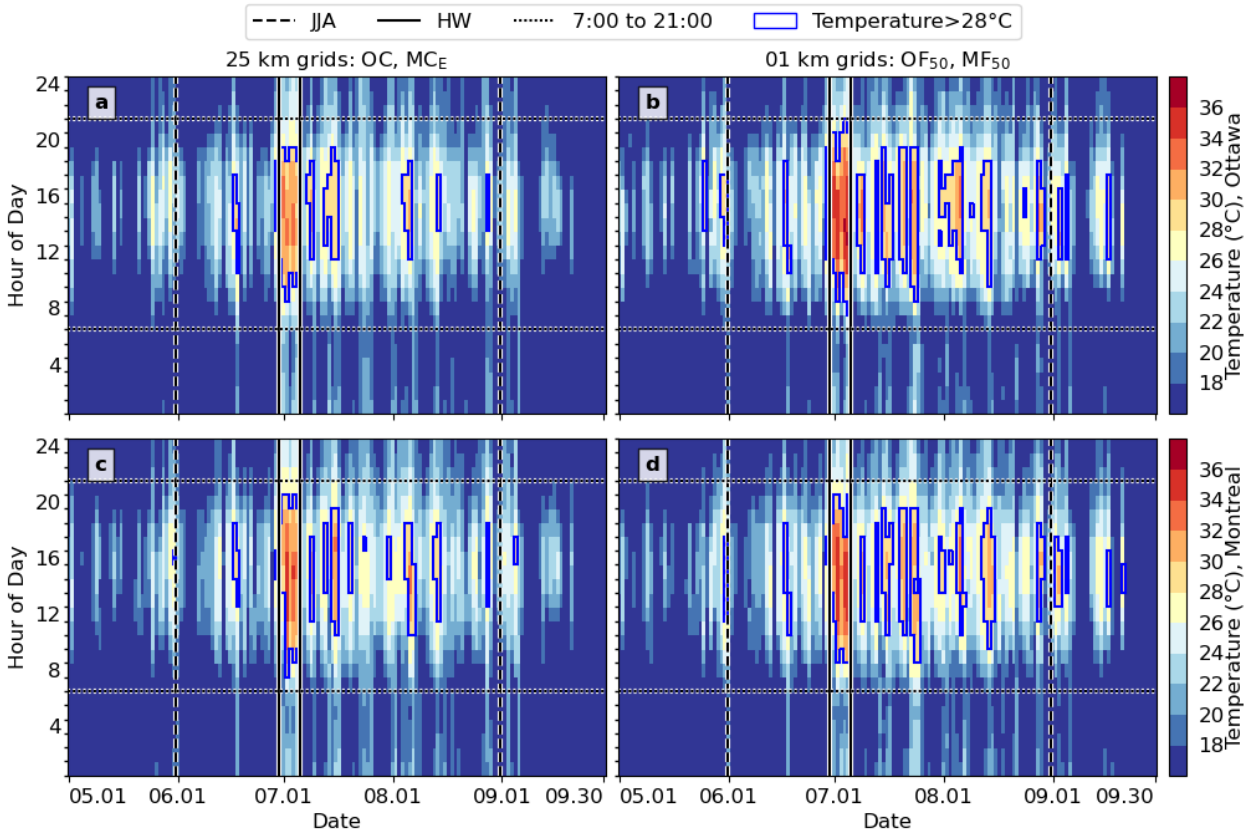

Figure 7. The hourly distribution of the outdoor air temperature of simulations completed at 1 and 25 km grid resolution at 50th percentile urban location in Ottawa and Montreal. (HW: heatwave period from June 30 to July 5, 2018 shown with vertical solid lines; JJA: June, July and August shown with vertical dashed lines)

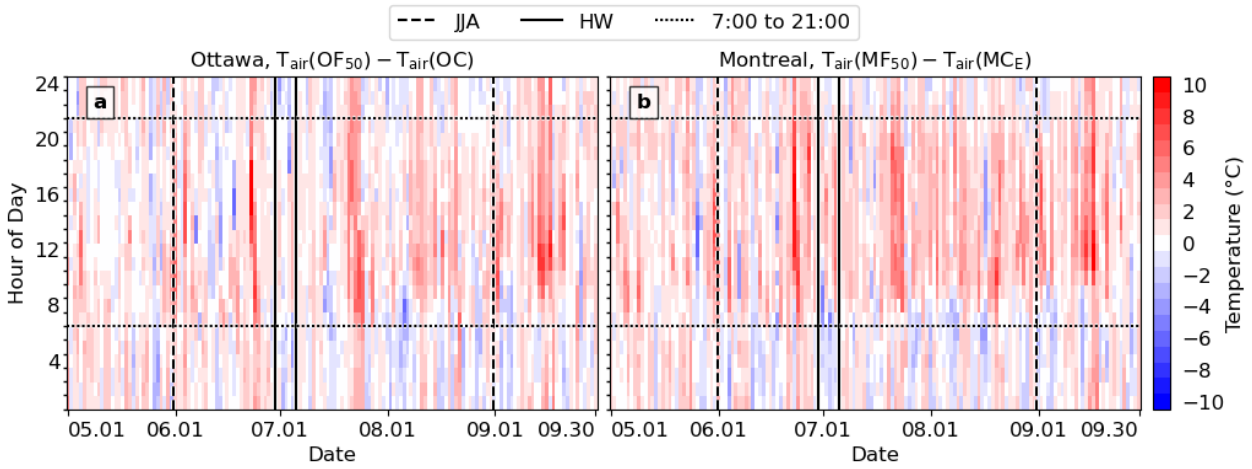

Figure 8. The hourly difference in outdoor air temperature from simulations completed at 1 and 25 km grid resolution at 50th percentile urban location in Ottawa and Montreal. (HW: heatwave period from June 30 to July 5, 2018 shown with vertical solid lines; JJA: June, July and August shown with vertical dashed lines)

3.3. Indoor overheating from simulations completed at 1 and 25 km grid resolution

The outdoor conditions at the selected representative grids from simulations completed at 1 and 25 km using the WRF model were used as inputs into the EnergyPlus program to simulate the indoor environment in the archetype single-detached home. As mentioned before, indoor overheating is calculated using operative temperatures instead of air temperatures for the outdoor overheating assessment. The results are shown in Table 7-8 and Figures 9-10. The indoor operative temperatures were found to be higher than the outdoor air temperatures by about 8-10 ºC, and the percentage of overheating hours ($POH_{28^\circ C}$) with temperatures more than 28ºC are found to be 2-3 times greater than those from the outdoor overheating analysis, so the building undergoes a much longer overheating period than that evident for the outdoors.

Between the different sections of the single-detached home, higher temperatures and overheating conditions are found in the bedroom (located on the 1st floor) than in the living room (located on the ground floor). This is likely because of the thermal stratification effect in buildings when warmer air circulates and moves from the lower to upper spaces. The comparison of Tables 7 and 8 shows that the operative temperatures in the bedroom are up to 1ºC higher, which, together with a lower threshold (26 ºC) for the calculation of overheating in the bedroom, leads to about 45% more overheating hours than in the living room. Since occupants often spend more time in the bedroom than the living room, this potentially creates high overheating risks. In addition, the temperature difference was found higher during the day than during the night.

Finally, indoor overheating obtained from simulations completed at 1 and 25 km resolution, and their relative difference is investigated. The timing of the EHE during June 30-July 5, 2018, is well captured in the indoor temperatures from both simulations completed at 1 and 25 km resolution, as shown by Figure 9. It shows the indoor operative temperatures in the living room for the 50th percentile urban location however, its magnitude was underestimated in the results of simulations completed at 25 km simulation resolution. In line with the observations made from the outdoor overheating assessment, the operative temperatures and percentage of overheating hours from the simulations completed at 25 km resolution fall between the 0th and 5th quantile urban grids in both cities, again highlighting that indoor overheating at more than 95% of the urban grids is underpredicted if simulations completed at 25 km resolution are used for the assessment. This is also reflected from the difference in the number of overheating hours obtained at, for example, the 50th percentile grid. Our results indicate that about 80% of hours in Ottawa and 73% of hours in Montreal over the time period of analysis are simulated with higher temperatures from simulations completed at 1 km than the 25 km resolution. The difference in mean operative temperature

between simulations completed at 1 and 25 km resolution is slightly lower than the difference obtained in terms of outdoor air temperatures; however, the percentage of overheating hours is comparable.

Table 7. Summary of thermal conditions in the living room of the archetype single-detached house building simulated at representative grids from simulations completed at 1 and 25 km grid resolution

Climate statistic	Ottawa grids						Montreal grids						
	OC	OF_0	OF_5	OF_{50}	OF_{95}	OF_{100}	MC_W	MC_E	MF_0	MF_5	MF_{50}	MF_{95}	MF_{100}
$T_{opt,mean}$ (°C)	25.7	24.9	26.0	26.3	26.3	26.4	25.7	25.8	24.7	26.0	26.2	26.3	26.4
$T_{opt,mean}^{day}$ (°C)	26.2	25.3	26.6	27.0	27.0	27.1	26.3	26.4	25.2	26.7	26.9	27.0	27.1
$T_{opt,mean}^{night}$ (°C)	24.7	24.2	24.9	25.1	25.1	25.2	24.8	24.8	24.0	24.9	25.1	25.2	25.2
$T_{opt,max}$ (°C)	34.9	28.7	35.9	37.0	36.6	37.3	35.9	36.7	28.7	36.6	36.7	37.4	37.6
$POH_{28°C}$ (%)	9.2	0.2	12.8	16.2	16.9	17.6	8.6	9.4	0.1	12.6	15.7	16.3	17.5
$POH_{28°C}^{day}$ (%)	14.5	0.3	19.9	25.2	26.1	27.0	13.2	14.3	0.1	19.9	24.1	24.9	26.8
$POH_{28°C}^{night}$ (%)	0.4	0.0	1.1	1.2	1.7	1.8	0.9	1.2	0.0	0.3	1.5	2.0	2.1

Table 8. Summary of thermal conditions in the bedroom of the archetype single-detached house building simulated at representative grids from simulations completed at 1 and 25 kmgrid resolution .

Climate statistic	Ottawa grids						Montreal grids						
	OC	OF_0	OF_5	OF_{50}	OF_{95}	OF_{100}	MC_W	MC_E	MF_0	MF_5	MF_{50}	MF_{95}	MF_{100}
$T_{opt,mean}$ (°C)	26.2	25.4	26.6	26.8	26.9	27.0	26.2	26.3	25.2	26.6	26.8	26.9	27.0
$T_{opt,mean}^{day}$ (°C)	26.7	25.7	27.2	27.5	27.6	27.7	26.8	26.8	25.5	27.3	27.5	27.5	27.7
$T_{opt,mean}^{night}$ (°C)	25.3	24.8	25.5	25.7	25.7	25.8	25.4	25.4	24.7	25.5	25.7	25.8	25.8
$T_{opt,max}$ (°C)	35.9	29.8	37.0	38.1	37.7	38.3	37.0	37.7	30.8	37.9	37.8	38.6	38.7

$POH_{26°C}$ (%)	48.9	35.0	56.7	61.0	62.8	64.1	49.7	50.3	28.2	58.6	60.0	61.9	62.3
$POH_{26°C}^{day}$ (%)	60.0	46.3	67.6	71.9	73.4	74.3	60.7	61.6	37.2	69.8	70.4	71.8	72.5
$POH_{26°C}^{night}$ (%)	30.2	16.3	38.5	42.9	45.0	47.0	31.5	31.4	13.2	39.8	42.6	45.4	45.5

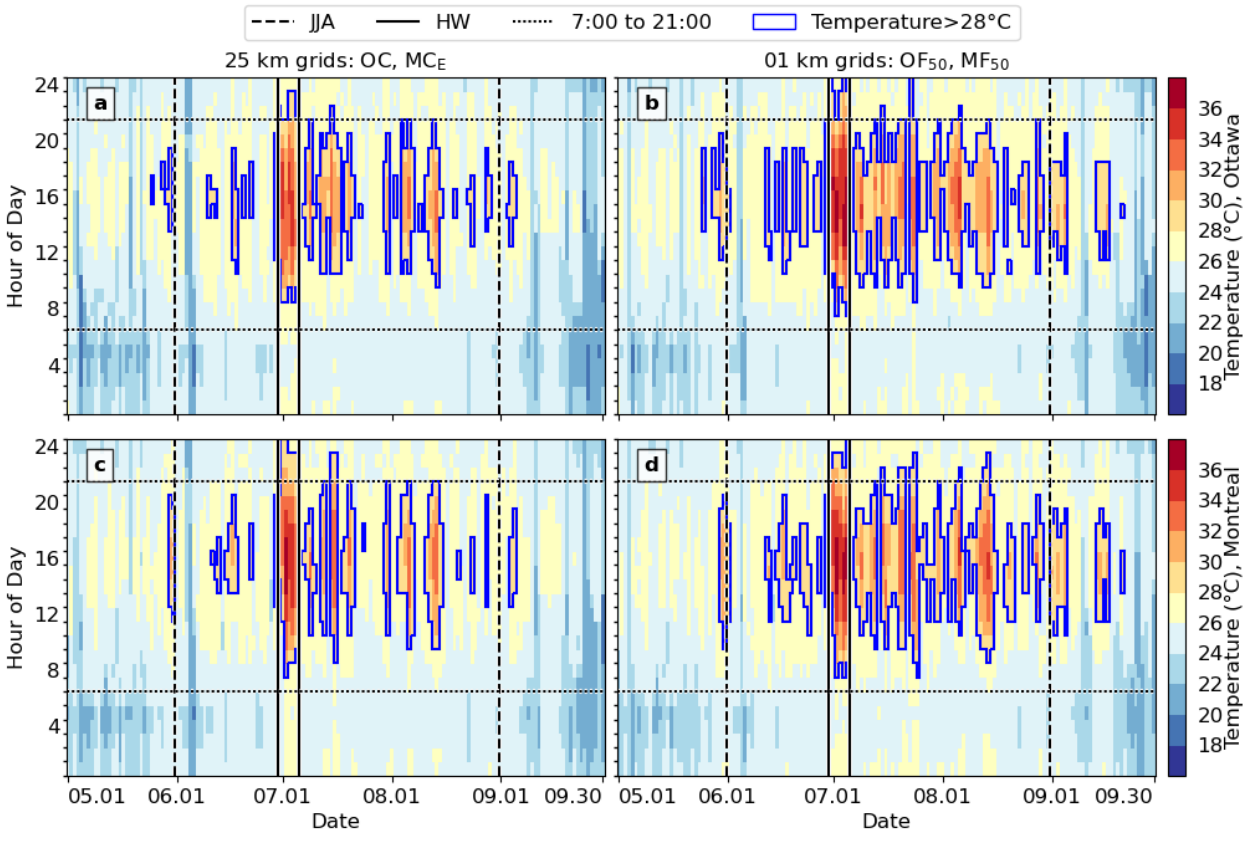

Figure 9. The hourly distribution of the indoor operative temperature in the living room from simulations completed at 1 and 25 km grid resolution at 50th percentile urban location in Ottawa and Montreal. (HW: heatwave period from June 30 to July 5, 2018 shown with vertical solid lines; JJA: June, July and August shown with vertical dashed lines)

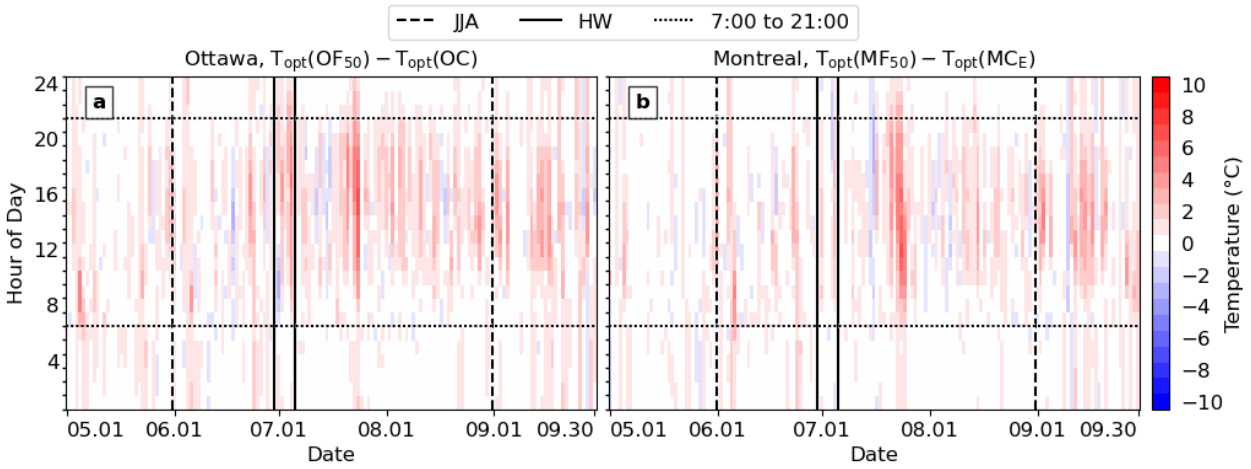

Figure 10. The hourly difference in indoor operative temperature in the living room from simulations completed at 1 and 25 km grid resolution at 50th percentile urban location in Ottawa and Montreal. (HW: heatwave period from June 30 to July 5, 2018 shown with vertical solid lines; JJA: June, July and August shown with vertical dashed lines)

4. Conclusions

This study highlights the added value of using high-resolution convection-permitting climate data over regional climate model (RCM) simulated data for the overheating assessment in cities. The study was conducted for two major Canadian cities: Ottawa and Montreal, over a period ranging between May and September 2018. Urban climate simulations were performed at a convection-permitting spatial resolution of 1 km, and at a typical RCM spatial resolution of 25 km using a Weather Research and Forecasting (WRF) model. The magnitude of overheating as occurred outdoors and within a single-detached home were evaluated by using the two sets of climate data completed at either grid resolution.

The results demonstrate greater accuracy from simulations undertaken at a 1 km grid resolution when modelling the outdoor climate than that obtained at a 25 km resolution by comparing with

the observation at nine weather stations in the domain. The air temperature is underestimated in simulations for both 1 and 25 km resolution, whereas simulations completed at a 1 km resolution have smaller bias, mean absolute error, and root mean squared error than those done at 25 km. The added accuracy of 1 km simulations in modelling extreme hight temperatures is especially evident from the validation results.

The temporal variation in air temperatures over the time period of the analysis (i.e. June 30 – July 05, 2018) is well captured in simulations undertaken at both 1 km and 25 km grid resolution. However, the simulations done at a 25 km resolution are found to underpredict mean air temperatures by up to 2ºC over the entire study domain. The maximum air temperatures are underpredicted by up to 3ºC, and the number of overheating hours could be underpredicted by up to 200 hours, which is half the number of overheating hours predicted from the simulation completed at a 1 km resolution.

The indoor operative temperatures are found to be higher than the outdoor air temperatures by about 8-10 ºC, and the number of overheating hours with temperatures more than 28ºC is found to be 2-3 times greater than that obtained from the outdoor overheating analysis. The indoor overheating is also underestimated using the 25 km resolution climate data, at least 70% of hours over the time period of analysis are predicted with lower temperatures from simulations completed at 25 km than the median level of the 1 km resolution results.

The results from this study also permitted showing that, if simulations done at a 25 km grid resolution are used to assess outdoor and indoor overheating in the cities of Ottawa and Montreal, the extent of overheating in terms of modelled temperatures, their extremes, and the number of overheating hours can be underpredicted in about 95% of the urban area grids of both cities. These results highlight the importance completing urban climate simulations using convection-

permitting climate data as compared to regional climate models for outdoor and indoor overheating analysis in cities. In the face of rapid urbanization and climate change, it is essential that future projected overheating effects are quantified in the urban centres of cities for different urban growth and climate change scenarios by conducting convection-permitting climate simulations from which heat-stress mitigation strategies can be developed in the future.

Acknowledgments

The research described in this paper was supported by the Natural Sciences and Engineering Research Council (NSERC) of Canada through the Advancing Climate Change Science in Canada Program [#ACCPJ 535986 - 18] as well as funding from Infrastructure Canada by the means of Climate Resilient Buildings and Core Public Infrastructure project. This research was aslo made possible, in part, by Calcul Québec (www.calculquebec.ca) and Compute Canada (www.computecanada.ca).

References

[1] G.A. Meehl, C. Tebaldi, More intense, more frequent, and longer lasting heat waves in the 21st century, Science (80-.). 305 (2004) 994–997. https://doi.org/10.1126/science.1098704.

[2] World Meteorological Organization (WMO), World Health Organization (WHO), Heatwaves and Health: Guidance on Warning-System Development, 2015. http://www.who.int/globalchange/publications/WMO_WHO_Heat_Health_Guidance_2015.pdf.

[3] M. Santamouris, C. Cartalis, A. Synnefa, Local urban warming , possible impacts and a resilience plan to climate change for the historical center of Athens , Greece, Sustain. Cities Soc. 19 (2015) 281–291. https://doi.org/10.1016/j.scs.2015.02.001.

[4] CIBSE, The limits of thermal comfort : avoiding overheating in European buildings, 2013. https://doi.org/10.1017/CBO9781107415324.004.

[5] T.R. Oke, The energetic basis of the urban heat island (Symons Memorial Lecture, 20 May 1980)., Q. Journal, R. Meteorol. Soc. 108 (1982) 1–24. http://www.scopus.com/inward/record.url?eid=2-s2.0-0020371056&partnerID=40&md5=693696300a399c5179461d96ba5026d7.

[6] F. Giorgi, Thirty Years of Regional Climate Modeling: Where Are We and Where Are We Going next?, J. Geophys. Res. Atmos. 124 (2019) 5696–5723. https://doi.org/10.1029/2018JD030094.

[7] D.P. Dee, S.M. Uppala, A.J. Simmons, P. Berrisford, P. Poli, S. Kobayashi, U. Andrae, M.A. Balmaseda, G. Balsamo, d P. Bauer, The ERA-Interim reanalysis: Configuration and performance of the data assimilation system, Q. J. R. Meteorol. Soc. 137 (2011) 553–597.

[8] F. Mesinger, G. DiMego, E. Kalnay, K. Mitchell, P.C. Shafran, W. Ebisuzaki, D. Jovic, J. Woolen, E. Rogers, E.H. Berbery, North American regional reanalysis. Bulletin of the American Meteorological Society, Am. Meteorol. Soc. 87 (2006) 343–360.

[9] S. Saha, S. Moorthi, H.-L. Pan, X. Wu, J. Wang, S. Nadiga, P. Tripp, R. Kistler, J. Woollen, D. Behringer, The NCEP climate forecast system reanalysis, Bull. Am. Meteorol. Soc. 91 (2010) 1015–1058.

[10] F. Giorgi, W.J. Gutowski Jr, Regional dynamical downscaling and the CORDEX initiative, Annu. Rev. Environ. Resour. 40 (2015) 467–490.

[11] A. Di Luca, R. de Elía, R. Laprise, Challenges in the quest for added value of regional climate dynamical downscaling, Curr. Clim. Chang. Reports. 1 (2015) 10–21.

[12] P. Lucas-Picher, R. Laprise, K. Winger, Evidence of added value in North American regional climate model hindcast simulations using ever-increasing horizontal resolutions, Clim. Dyn. 48 (2017) 2611–2633. https://doi.org/10.1007/s00382-016-3227-z.

[13] A. Martynov, R. Laprise, L. Sushama, K. Winger, L. Šeparović, B. Dugas, Reanalysis-driven climate simulation over CORDEX North America domain using the Canadian Regional Climate Model, version 5: model performance evaluation, Clim. Dyn. 41 (2013) 2973–3005.

[14] L. Šeparović, A. Alexandru, R. Laprise, A. Martynov, L. Sushama, K. Winger, K. Tete, M. Valin, Present climate and climate change over North America as simulated by the fifth-generation Canadian regional climate model, Clim. Dyn. 41 (2013) 3167–3201.

[15] L. Qiu, E.-S. Im, J. Hur, K.-M. Shim, Added value of very high resolution climate simulations over South Korea using WRF modeling system, Clim. Dyn. 54 (2020) 173–189.

[16] S. Mayer, C.F. Maule, S. Sobolowski, O.B. Christensen, H.J.D. Sørup, M.A. Sunyer, K. Arnbjerg-Nielsen, I. Barstad, Identifying added value in high-resolution climate simulations over Scandinavia, Tellus, Ser. A Dyn. Meteorol. Oceanogr. 67 (2015) 1–18. https://doi.org/10.3402/tellusa.v67.24941.

[17] C.L. Curry, B. Tencer, K. Whan, A.J. Weaver, M. Giguère, E. Wiebe, Searching for Added Value in Simulating Climate Extremes with a High-Resolution Regional Climate Model over Western Canada, Atmos. - Ocean. 54 (2016) 364–384. https://doi.org/10.1080/07055900.2016.1158146.

[18] D. Caya, R. Laprise, A semi-implicit semi-Lagrangian regional climate model: The Canadian RCM, Mon. Weather Rev. 127 (1999) 341–362. https://doi.org/10.1175/1520-0493(1999)127<0341:asislr>2.0.co;2.

[19] A.F. Prein, W. Langhans, G. Fosser, A. Ferrone, N. Ban, K. Goergen, M. Keller, M. Tölle, O. Gutjahr, F. Feser, E. Brisson, S. Kollet, J. Schmidli, N.P.M. Van Lipzig, R. Leung, A review on regional convection-permitting climate modeling: Demonstrations, prospects, and challenges, Rev. Geophys. 53 (2015) 323–361. https://doi.org/10.1002/2014RG000475.

[20] K. Mahoney, M.A. Alexander, G. Thompson, J.J. Barsugli, J.D. Scott, Changes in hail and flood risk in high-resolution simulations over Colorado's mountains, Nat. Clim. Chang. 2 (2012) 125–131.

[21] K. Mahoney, M. Alexander, J.D. Scott, J. Barsugli, High-resolution downscaled simulations of warm-season extreme precipitation events in the Colorado Front Range under past and future climates, J. Clim. 26 (2013) 8671–8689.

[22] A.F. Prein, G.J. Holland, R.M. Rasmussen, J. Done, K. Ikeda, M.P. Clark, C.H. Liu, Importance of regional climate model grid spacing for the simulation of heavy precipitation in the Colorado headwaters, J. Clim. 26 (2013) 4848–4857.

[23] A.F. Prein, A. Gobiet, M. Suklitsch, H. Truhetz, N.K. Awan, K. Keuler, G. Georgievski, Added value of convection permitting seasonal simulations, Clim. Dyn. 41 (2013) 2655–2677.

[24] R. Rasmussen, K. Ikeda, C. Liu, D. Gochis, M. Clark, A. Dai, E. Gutmann, J. Dudhia, F. Chen, M. Barlage, Climate change impacts on the water balance of the Colorado headwaters: High-resolution regional climate model simulations, J. Hydrometeorol. 15 (2014) 1091–1116.

[25] W. Langhans, J. Schmidli, O. Fuhrer, S. Bieri, C. Schär, Long-term simulations of thermally driven flows and orographic convection at convection-parameterizing and cloud-resolving resolutions, J. Appl. Meteorol. Climatol. 52 (2013) 1490–1510.

[26] G. Fosser, S. Khodayar, P. Berg, Benefit of convection permitting climate model simulations in the representation of convective precipitation, Clim. Dyn. 44 (2015) 45–60.

[27] N. Ban, J. Schmidli, C. Schär, Evaluation of the convection-resolving regional climate modeling approach in decade-long simulations, J. Geophys. Res. Atmos. 119 (2014) 7889–7907.

[28] S.C. Chan, E.J. Kendon, H.J. Fowler, S. Blenkinsop, C.A.T. Ferro, D.B. Stephenson, Does increasing the spatial resolution of a regional climate model improve the simulated daily precipitation?, Clim. Dyn. 41 (2013) 1475–1495.

[29] C. Hohenegger, P. Brockhaus, C. Schar, Towards climate simulations at cloud-resolving scales, Meteorol. Zeitschrift. 17 (2008) 383–394.

[30] T. Mölg, G. Kaser, A new approach to resolving climate-cryosphere relations: Downscaling

climate dynamics to glacier-scale mass and energy balance without statistical scale linking, J. Geophys. Res. Atmos. 116 (2011).

[31] H.L. Cloke, F. Pappenberger, Ensemble flood forecasting: A review, J. Hydrol. 375 (2009) 613–626.

[32] J. Bartholmes, E. Todini, Coupling meteorological and hydrological models for flood forecasting, Hydrol. Earth Syst. Sci. Discuss. 9 (2005) 333–346.

[33] A.M. Foley, P.G. Leahy, A. Marvuglia, E.J. McKeogh, Current methods and advances in forecasting of wind power generation, Renew. Energy. 37 (2012) 1–8.

[34] J. Kleissl, Solar energy forecasting and resource assessment, Academic Press, 2013.

[35] M.H. Tölle, O. Gutjahr, G. Busch, J.C. Thiele, Increasing bioenergy production on arable land: Does the regional and local climate respond? Germany as a case study, J. Geophys. Res. Atmos. 119 (2014) 2711–2724.

[36] K. Van Weverberg, K. De Ridder, A. Van Rompaey, Modeling the contribution of the Brussels heat island to a long temperature time series, J. Appl. Meteorol. Climatol. 47 (2008) 976–990.

[37] W.C. Skamarock, J.B. Klemp, J. Dudhia, D.O. Gill, Z. Liu, J. Berner, W. Wang, J.G. Powers, M.G. Duda, D.M. Barker, X.-Y. Huang, A Description of the Advanced Research WRF Model Version 4, Boulder, Colorado, USA, 2019. http://library.ucar.edu/research/publish-technote.

[38] S. Grossman-Clarke, J.A. Zehnder, T. Loridan, C.S.B. Grimmond, Contribution of land use changes to near-surface air temperatures during recent summer extreme heat events in the

Phoenix metropolitan area, J. Appl. Meteorol. Climatol. 49 (2010) 1649–1664. https://doi.org/10.1175/2010JAMC2362.1.

[39] H. Wouters, K. De Ridder, M. Demuzere, D. Lauwaet, N.P.M. Van Lipzig, The diurnal evolution of the urban heat island of Paris: a model-based case study during Summer 2006, Atmos. Chem. Phys. 13 (2013) 8525–8541.

[40] M. Xue, K.K. Droegemeier, V. Wong, The Advanced Regional Prediction System (ARPS)–A multi-scale nonhydrostatic atmospheric simulation and prediction model. Part I: Model dynamics and verification, Meteorol. Atmos. Phys. 75 (2000) 161–193.

[41] M. Xue, K.K. Droegemeier, V. Wong, A. Shapiro, K. Brewster, F. Carr, D. Weber, Y. Liu, D. Wang, The Advanced Regional Prediction System (ARPS)–A multi-scale nonhydrostatic atmospheric simulation and prediction tool. Part II: Model physics and applications, Meteorol. Atmos. Phys. 76 (2001) 143–165.

[42] H. Taha, Meso-urban meteorological and photochemical modeling of heat island mitigation, Atmos. Environ. 42 (2008) 8795–8809.

[43] S. Schubert, S. Grossman-Clarke, The Influence of green areas and roof albedos on air temperatures during Extreme Heat Events in Berlin, Germany, Meteorol. ZEITSCHRIFT. 22 (2013) 131–143. https://doi.org/10.1127/0941-2948/2013/0393.

[44] V. Ciancio, S. Falasca, I. Golasi, G. Curci, M. Coppi, F. Salata, Influence of input climatic data on simulations of annual energy needs of a building: Energyplus and WRF modeling for a case study in Rome (Italy), Energies. 11 (2018). https://doi.org/10.3390/en11102835.

[45] U.S. Department of Energy's, Building Technologies Office, EnergyPlus 2020, (2020).

https://energyplus.net/.

[46] R. Jain, X. Luo, G. Sever, T. Hong, C. Catlett, Representation and evolution of urban weather boundary conditions in downtown Chicago, J. Build. Perform. Simul. 13 (2020) 182–194. https://doi.org/10.1080/19401493.2018.1534275.

[47] X. Luo, P. Vahmani, T. Hong, A. Jones, City-scale building anthropogenic heating during heat waves, Atmosphere (Basel). 11 (2020). https://doi.org/10.3390/atmos11111206.

[48] ECCC, Canada's top 10 weather stories of 2018., (2019). https://www.canada.ca/en/environment-climate-change/services/top-ten-weather-stories/2018.html#toc1.

[49] Environment and Climate Change Canada, Glossary - Climate - Environment and Climate Change Canada, Climate.Weather.Gc.Ca. (n.d.). https://climate.weather.gc.ca/glossary_e.html.

[50] F. Lamothe, M. Roy, S.-É. Racine-Hamel, Enquête épidémiologique - Vague de chaleur à l'été 2018 à Montréal, Montréal, Québec, 2019. https://doi.org/9782550840206.

[51] North American Land Change Monitoring System (NALCMS) dataset, 2015, (2015).

[52] National Centers for Environmental Prediction, National Weather Service, NOAA, U.S. Department of Commerce, NCEP North American Regional Reanalysis (NARR), (2005). https://rda.ucar.edu/datasets/ds608.0/.

[53] A. Gaur, M. Lacasse, M. Armstrong, H. Lu, C. Shu, A. Fields, F.S. Palou, Y. Zhang, Effects of using different urban parametrization schemes and land-cover datasets on the accuracy of WRF model over the City of Ottawa, Urban Clim. 35 (2021) 100737.

https://doi.org/10.1016/j.uclim.2020.100737.

[54] S.Y. Hong, J. Dudhia, S.H. Chen, A revised approach to ice microphysical processes for the bulk parameterization of clouds and precipitation, Mon. Weather Rev. 132 (2004) 103–120. https://doi.org/10.1175/1520-0493(2004)132<0103:ARATIM>2.0.CO;2.

[55] F. Chen, J. Dudhia, Coupling an advanced land surface-hydrology model with the Penn-State-NCAR MM5 modeling system. Part I : Model Implementation and Sensitivity, Mon. Weather Rev. 129 (2001) 569–585.

[56] Z.I. Janjić, The Step-Mountain Eta Coordinate Model: Further Developments of the Convection, Viscous Sublayer, and Turbulence Closure Schemes, Mon. Weather Rev. 53 (1994) 927–945. https://doi.org/https://doi.org/10.1175/1520-0493(1994)122<0927:TSMECM>2.0.CO;2.

[57] J. Dudhia, Numerical study of convection observed during the winter monsoon experiment using a mesoscale two-dimensional model, J. Atmos. Sci. 46 (1989) 3077–3107.

[58] E.J. Mlawer, S.J. Taubman, P.D. Brown, M.J. Iacono, S.A. Clough, Radiative transfer for inhomogeneous atmospheres: RRTM, a validated correlated-k model for the longwave, J. Geophys. Res. D Atmos. 102 (1997) 16663–16682. https://doi.org/10.1029/97jd00237.

[59] J.S. Kain, The Kain–Fritsch Convective Parameterization: An Update, J. Appl. Meteorol. 43 (2004) 170–181.

[60] A. Martilli, A. Clappier, M.W. Rotach, An urban surface exchange parameterisation for mesoscale models, Boundary-Layer Meteorol. 104 (2002) 261–304.

[61] ECCC, Historical weather data, Canada, (n.d.).

https://climate.weather.gc.ca/historical_data/search_historic_data_e.html.

[62] A. Parekh, Representative Housing Thermal Archetypes for Energy Analysis Models, Ottawa, ON, Canada, 2012.

[63] National Research Council of Canada, National Building Code of Canada, 2015.

[64] CIBSE, Environmental design CIBSE: Guide A, 2011. http://www.cambeep.eng.cam.ac.uk/References/cibse.

[65] National Research Council of Canada, National Energy Code of Canada for Buildings 2017, (2017).

[66] A. Gaur, M. Lacasse, M. Armstrong, Climate Data to Undertake Hygrothermal and Whole Building Simulations Under Projected Climate Change Influences for 11 Canadian Cities, Data. 4 (2019) 72. https://doi.org/10.3390/data4020072.

[67] A. Laouadi, M. Bartko, M.A. Lacasse, A new methodology of evaluation of overheating in buildings, Energy Build. 226 (2020) 110360. https://doi.org/10.1016/j.enbuild.2020.110360.

[68] K.J. Lomas, R. Giridharan, Thermal comfort standards, measured internal temperatures and thermal resilience to climate change of free-running buildings: A case-study of hospital wards, Build. Environ. 55 (2012) 57–72. https://doi.org/10.1016/j.buildenv.2011.12.006.

[69] K.J. Lomas, S.M. Porritt, Overheating in buildings: lessons from research, Build. Res. Inf. 45 (2017) 1–18. https://doi.org/10.1080/09613218.2017.1256136.

[70] CIBSE, Design Summer Years for London, Tech. Memo. 49. (2014) 1–29.

[71] Department of Health, Heating and ventilation systems. Health Technical Memorandum 03-01: Specialised ventilation for healthcare premises. Part A: Design and validation., 2007.

[72] Zero Carbon Hub, Defining overheating, (2015) 21. https://doi.org/http://www.zerocarbonhub.org/sites/default/files/resources/reports/ZCH-OverheatingEvidenceReview-Definitions.pdf.

[73] Zero Carbon Hub, Assessing overheating risk, 2015.

Appendix

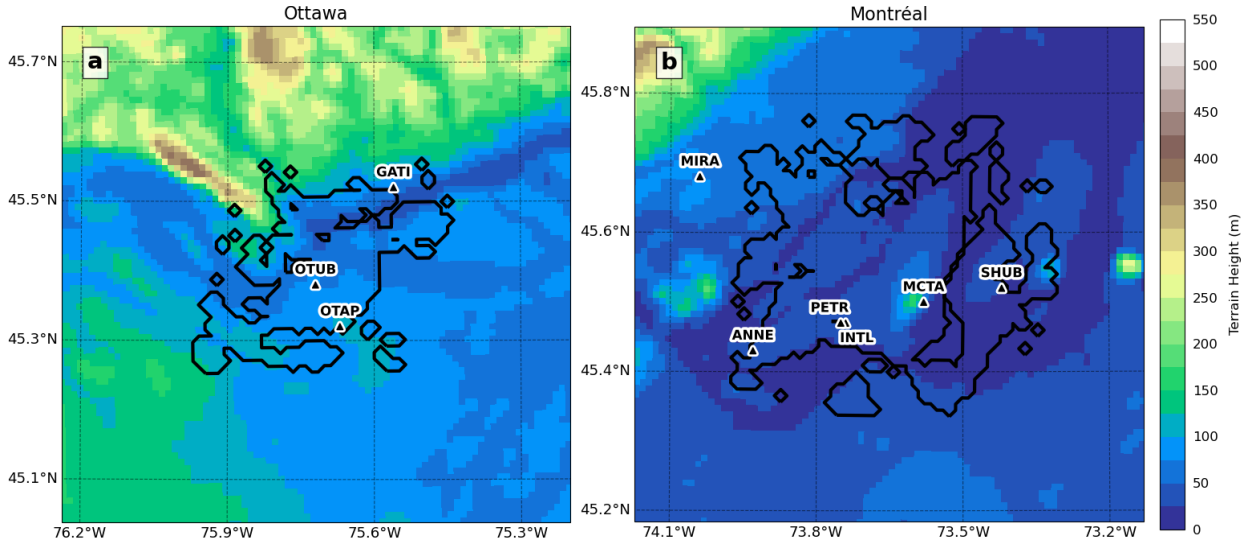

Figure A1. Terrain height distribution and the climate gauging stations around the Ottawa and Montreal cities.